ACS APPLIED BIO MATERIALS

www.acsabm.org

Article

Inactivation of Vesicular Stomatitis Virus with Light-Activated Carbon Dots and Mechanistic Implications

Audrey F. Adcock, Ping Wang, Isaiah S. Ferguson, Somtochukwu C. Obu, Ya-Ping Sun,* and Liju Yang*

Cite This: *ACS Appl. Bio Mater.* 2022, 5, 3158−3166

Read Online

ACCESS | Metrics & More | Article Recommendations | Supporting Information

ABSTRACT: The prevention of viral transmission is an important step to address the spread of viral infections. Using the enveloped vesicular stomatitis virus (VSV) as a model, this study explored the antiviral functions of the specifically designed and prepared carbon dots (CDots). The CDots were prepared using small carbon nanoparticles with surface functionalization−passivation by oligomeric polyethylenimine (PEI). The results indicated that the PEI-CDots were readily activated by visible light to effectively and efficiently inactivate VSVs under various combinations of experimental conditions (viral titer, dot concentration, and treatment time). The photodynamically induced viral structural protein degradation and genomic RNA degradation were observed, suggesting the mechanistic origins, leading to the inactivation of virus. The results suggested CDots as a class of promising broad-spectrum antiviral agents for disinfection of viruses.

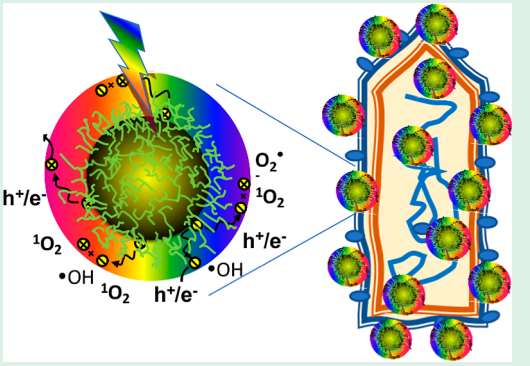

KEYWORDS: *carbon dots, light-activated, inactivation, virus, mechanism, vesicular stomatitis virus*

INTRODUCTION

The wide spread of viral infections and the associated morbidity and mortality have raised enormous concerns in public health worldwide.[1] Especially, the current global pandemic of the coronavirus SARS-CoV-2[2,3] has caused more than 400 million infections and more than 5 million death as of February 2022, with major effects on public health, economy, and the society. The pandemic is still on-going, and the number of infections is increasing with new variants continuously emerging.[4] Not long ago, emerging viruses, Ebola, also caused deadly infectious diseases. Besides this current and past global emergences caused by emerging viruses, many other viruses are co-existing with human and can cause deadly infectious diseases as well. For example, the influenza or "the flu" is perhaps the most familiar virus that causes respiratory infections.[5] Indeed, these viral infections are responsible for about one-third of the total deaths caused by infectious diseases.[6] The wide impacts of viral infections on the society highlight the need for the development of effective antiviral strategies and especially stimulate the extensive search for broad-spectrum antiviral strategies/agents that are applicable for rapid response or repurposing to combat emerging viruses.

Viruses have different structures, replicate in a different way from bacteria, and are generally not responsive to antibiotics. The best practice to prevent viral infection is vaccination, though only a limited number of vaccines are available, and constant antigenic shift in some viruses also creates difficulties for vaccine development. In many cases, hygiene and sanitation practices are the most effective strategies for the control of viral infections. Therefore, development of antiviral agents for the effective inactivation of viruses in various settings is one of the practical ways for preventing viral transmission and spreading. In this regard, many well-known chemical and physical methods effective for inactivating bacterial pathogens have been extended for direct inactivation of viruses.[7−22]

Antimicrobial photodynamic inactivation (PDI) has been pursued as a suitable approach for disinfection purpose, gaining more popularity in recent years with the use of new non-traditional photosensitizers. Carbon dots (CDots) have emerged to be recognized as a new class of photoactive nanomaterials that can be activated by visible light to exhibit excellent antimicrobial activities against a broad range of different bacterial species, including multi-drug resistant species.[23−25] However, there have only been a few studies on the antiviral function of CDots based on diverse properties/functions of CDots[26−32] but rarely on the photodynamic property of CDots. Our groups reported that CDots exhibited photo-activated antiviral activity to model MS2 bacterial phage, diminishing the infectivity of bacteriophage MS2 to its host cells due to the oxidation of viral proteins and the

Received: February 19, 2022
Accepted: June 27, 2022
Published: July 7, 2022

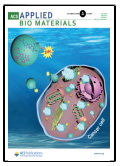

https://doi.org/10.1021/acsabm.2c00153
ACS Appl. Bio Mater. 2022, 5, 3158−3166

degradation of viral genomic RNA by the treatment with light-activated CDots.[29]

Many viruses that spread widely are enveloped, such as respiratory viruses, herpes, hepatitis, and HIV. Enveloped viruses possess a capsid consisted of a lipid bilayer which is originated from the lipids of the host cell. Therefore, different viruses could have similar lipid part of the envelope,[33] which might be an excellent target for broad-spectrum antiviral agents.[34,35] Since the oxidation of unsaturated lipids by reactive species such as singlet molecular oxygen is well established,[36,37] PDI of enveloped viruses represents a viable approach. CDots upon photoexcitation are known to produce highly reactive species responsible for the observed antimicrobial activities.[29,30] Their effective inactivation of enveloped viruses deserves investigations.

In this study, vesicular stomatitis virus (VSV), a negative-sense, single-stranded RNA, enveloped virus, was selected as a model for the study on the effect of CDots coupled with visible light on viral inactivation. VSV in the *Rhabdoviridae* family is a bullet-shaped virus, generally 180 nm long and 75 nm wide. Its structure is significantly different from that of non-enveloped viruses, and it has been used as a representative enveloped virus in many studies aimed at the search for broad-spectrum antiviral agents and the associated mechanistic understanding,[38] especially for those agents that target the viral envelope. The structural differences between enveloped and non-enveloped viruses generally result in their different susceptibility or sensitivity to inactivation reagents/processes. In general, enveloped viruses tend to be of less resistance to desiccation and heat treatment, and they are easier to sterilize than non-enveloped viruses. In this regard, this study builds upon previous findings on antiviral activities of CDots with other virus models[29,31] to expand the investigation to VSV as a model of enveloped virus, aiming at the general applicability of CDots against a broader range of viruses with different structural variations, and the improved mechanistic understanding of the antiviral function of CDots with visible light.

MATERIALS AND METHODS

CDots. The CDots samples used in this study were prepared by the surface functionalization of pre-processed and selected small carbon nanoparticles with oligomeric polyethylenimine (PEI, average molecular weight ~ 600), denoted as PEI-CDots. Briefly, the small carbon nanoparticles were harvested from the commercially acquired carbon nano-powders (US Research Nanomaterials, Inc.) in procedures similar to those reported previously.[39,40] The nanoparticles were functionalized with PEI in the microwave-assisted thermal reactions by following the same processing protocols and conditions reported previously.[29,39,40] The resulting PEI-CDots were characterized by using NMR, microscopy, and optical spectroscopy techniques, from which the results were consistent with those of similarly prepared samples reported previously.[40] The PEI-CDots were in average sizes mostly 4−8 nm.[23] The aqueous solution of PEI-CDots had strong absorption within the visible spectrum that is similar to that of the aqueous suspended precursor.[23] Characterized by significant photon harvesting in the visible spectrum, the PEI-CDots also had strong fluorescence emission spectra in 450−650 nm with quantum yields (~20% at 400 nm excitation), comparable to those of other CDots reported previously.[24,25,29,39,40] The dot samples in aqueous solution were stored in the dark at room temperature and used for antiviral experiments. Information about the synthesis and characterization of PEI-CDots is provided in the Supporting Information.

VSV Virus Propagation and Purification. VSV, Indiana strain (VR-1238), and baby hamster kidney (BHK-21) cells (CCL-10) were purchased from ATCC (Manassas, VA). BHK-21 cells were cultured in high glucose Dulbecco's modified Eagle medium (DMEM) (Hyclone), supplemented with 10% FBS (HyClone) and no antibiotics, at 37 °C under a 5% CO_2 atmosphere. VSV was propagated in confluent monolayers of BHK-21 cells at a multiplicity of infection of 10. After the incubation at 37 °C for 1 h, DMEM supplemented with 2% FBS was added to the flask. Viruses were harvested approximately 18 h post inoculation by low-speed centrifugation at 5000*g* for 10 min to remove the cell debris.

To prepare the purified stock of VSV, the collected supernatant was centrifuged at 40,000*g* for 90 min at 4 °C using chilled Beckman rotor Type 70 Ti. The supernatant was discarded, and the pellet containing the VSV virus particles was resuspended in 3.5 mL of TNE buffer (Tris-EDTA (TE) buffer with NaCl) (100 mM NaCl, 10 mM Tris, 1 mM EDTA, pH 7.4). Then, 27 mL of 10% sucrose solution (w/v in NTE) was added to a centrifuge tube, and 3.5 mL of virus suspension solution was layered on the top of 10% sucrose. The total volume was adjusted to 37 mL by adding additional 6.5 mL of NTE. The sample was centrifuged at 150,000*g* for 1 h at 4 °C. The supernatant was removed, and the purified VSV pellet was resuspended in 2 mL of sterile deionized (DI) H_2O. The protein concentration was determined by the spectrophotometric measurement, and the final protein concentration of the VSV sample was set at 1 μg/mL. The purified VSV samples were stored at refrigeration until the viral titer could be determined by plaque assay and for further experimental uses.

VSV Virus Titration by Plaque Assay. The VSV titer was quantified by plaque assay in BHK-21 cells. Briefly, BHK-21 cells were seeded into six-well plates at a density of ~1 × 10^6 cells/well and incubated overnight to form confluent cell monolayers. The VSV samples were 1:10 serially diluted with DMEM without FBS, and aliquots of 400 μL of the dilution series were added to inoculate the BHK-21 cell monolayers. The plates were incubated for 1 h at 37 °C with gentle rocking every 10−15 min. After the infection, each well was overlaid with 1.2% agarose diluted 1:1 with DMEM supplemented with 2% FBS. After overnight incubation at 37 °C under a 5% CO_2 atmosphere, the cells were fixed with 4% formaldehyde solution and stained with 0.05% crystal violet in 20% methanol for plaque visualization and counting, to calculate the plaque-forming units per mL (PFU/mL).

CDots Treatment for VSV Inactivation. All CDots treatments for VSV viruses were carried out in 24-well plates. For dose-dependent tests, purified VSV particles at a concentration of ~10^8 PFU/mL (6 μL) were mixed with desired volumes of PEI-CDots to the final concentrations of CDots, ranging from 0.5 to 5 μg/mL in a total volume of 600 μL adjust by adding DI H_2O. Negative controls of VSV in sterile DI water without any PEI-CDots were also included in each experiment. The samples for each treatment were prepared in duplicates. Another plate was prepared in the same way but was wrapped in aluminum foil to block light and used as the controls of PEI-CDots treatment in the dark condition. Both plates were placed on an Orbital shaker (BT Lab Systems) with shaking at 330 rpm and exposed to visible light from a commercially acquired household daylight light-emitting diode (LED) bulb by CREE (17 W, omnidirectional 815 lumens) (Home Depot) placed at ~10 cm above the surface of the plates for a defined time period. The same light source and setting were used for all light exposure experiments to maintain consistent conditions.

For time-dependent tests, purified VSV particles at a concentration of ~10^8 PFU/mL (6 μL) were mixed with 5 μg/mL PEI-CDots in a total volume of 600 μL in each well. In the four different sets of treatment reactions, each set consisted of the sample of purified VSV particles mixed with 5 μg/mL PEI-CDots and a control VSV sample without CDots, and each set was maintained in duplicates. Another plate was prepared in the same way and was wrapped by aluminum foil for the dark control. Both plates were placed on the shaker and subjected to the same light exposure, as described above. At treatment time of 5, 15, 30, and 45 min, the treated samples were transferred to microtubes and protected from light by aluminum foil.

https://doi.org/10.1021/acsabm.2c00153
ACS Appl. Bio Mater. 2022, 5, 3158−3166

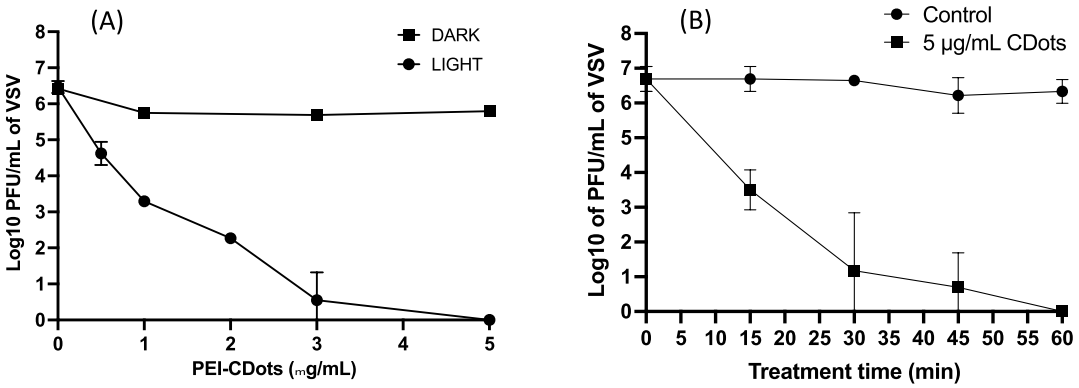

Figure 1. (A) Log reduction in virus titer when VSV samples were treated with PEI-CDots at concentrations, ranging from 0.5 to 5 μg/mL under visible light activation for 1 h, along with the corresponding CDots treatments in the dark condition; (B) log reduction in virus titer when VSV samples were treated with 5 μg/mL PEI-CDots under visible light activation for different treatment times, ranging from 15 to 60 min.

The CDots treatments to VSVs were stopped by restricting light exposure. After the treatments, each treated and control sample was immediately 1:10 serially diluted with DMEM. The viral titer in each sample was determined using plaque assay described above. Control samples without VSVs but with CDots concentrations equivalent to those in the serial dilutions were included as cytotoxicity controls to make sure no effect of CDots on the BHK-21 host cells. For all CDots treatment experiments, at least three independent tests were performed.

Analysis of VSV Viral Proteins by Sodium Dodecyl Sulfate−Polyacrylamide Gel Electrophoresis. For analyzing the structural proteins of VSV after CDots treatments, VSV samples containing higher viral titers were used. Purified VSV particles at a concentration of ~10^{10} PFU/mL (100 μL) were mixed with 10 μL of PEI-CDots at the desired concentration to reach the final concentrations at 20, 50, 100, and 200 μg/mL for 1 h exposure to the visible LED light using the same procedure as described above. The treated samples were wrapped in foil to protect from light.

To prepare samples for sodium dodecyl sulfate−polyacrylamide gel electrophoresis (SDS-PAGE) gel analysis, 5 μg of viral protein was mixed with one-quarter volume (2.5 μL) of 4× LDS sample buffer (Invitrogen, Carlsbad, CA), one-tenth volume (1 μL) of the 10× reducing agent (Invitrogen, Carlsbad, CA), in the final volume of 10 μL. The sample was heated at 70 °C for 10 min and then loaded in NuPage 4−12% bis−Tris gel at 10 μL/well. Each sample was used in duplicate. The gel was run using (3-(N-morpholino)propanesulfonic acid) (MOPS) running buffer (Life Technologies, Carlsbad, CA) at 200 V for 50 min. After the separation, the gel was washed three times with DI H_2O, each for 3−5 min. The gel was stained with GelCode Blue for 1 h and then destained by washing with 20 mL of DI H_2O twice. The images of the gels were captured using LI-COR Odyssey CLx and the Image Studio software version 5.2.

Analysis of VSV Genomic RNA by Agarose Gel. VSV particles at a concentration of ~10^{10} PFU/mL (225 μL) were mixed with 25 μL of the 100 μg/mL PEI-CDots under visible light for 1, 2, and 3 h. The controls were VSV particles mixed with DI H_2O. Viral genomic RNA was extracted from 250 μL of CDots-treated and the control VSV samples using the Invitrogen PureLink RNA/DNA Mini Kit (Thermo Fisher Scientific, Carlsbad, CA) according to the manufacturer's manual. The extracted RNA (5 μL) was mixed with 5 μL of 2× RNA sample buffer. The mixture was heated at 70 °C for 3 min and immediately transferred to ice. The samples were loaded at 10 μL/well in a 1.2% non-denaturing agarose gel, and the gel was run using TBE buffer at 100 V for 35 min. The gel was stained with 50 mL of 0.005% ethidium bromide solution for 30 min and then destained by washing twice with 50 mL DI H_2O for 5 min. The images of the gels were captured using the UVP Gel-DocIt^2 (Carestream Health, Inc., Rochester, NY), and the image analysis was performed using Image Studio v5.2 software.

ROS Scavenger Experiments. In order to confirm the generation of reactive oxygen species (ROS) during CDots treatment and to determine the sub-species of ROS, L-histidine and *tert*-butanol were used as scavengers for singlet molecular oxygen ($^1O_2$) and hydroxyl radicals ($^\bullet$OH), respectively. Experimentally, CDots treatments of VSV viruses were performed by using the similar setting described above but in the presence of scavengers. Briefly, VSV samples at a concentration of 10^8 to 10^9 PFU/mL were treated with a fixed PEI-CDots concentration (20 μg/mL) in the presence of either L-histidine or *tert*-butanol at varying concentrations of 30, 60, and 90 mM and exposed to the visible light for 1 h. Control samples included the untreated VSV samples, samples treated with PEI-CDots only, and samples treated with scavenger only. After the treatments, the viral titer in each sample was determined using the plaque assay described above. The comparison of the reductions in viral titer expressed as $\log_{10}$ of PFU/mL between the samples with PEI-CDots treatment in the presence and absence of L-histidine or *tert*-butanol provided information on the ROS species involved in the PDI of VSVs during CDots treatment.

RESULTS AND DISCUSSION

Inactivation of VSVs by CDots with Visible Light. For CDots treatment, purified VSVs at ~10^7 PFU/mL were mixed with PEI-CDots at various concentrations in the wells of a 24-well plate. The plate was placed on a shaker with consistent shaking at 330 rpm and exposed to visible light from a common household LED light bulb with the light intensity of ~7.8 mW/cm^2 at the samples and the wavelength spanning the entire visible light, ranging from ~400 to ~800 nm. Immediately following the treatment, the samples were diluted in a 1/10-fold series, and then, the dilutions were plated to inoculate BHK-21 monolayers in six-well plates at 400 μL/well to determine the virus titers in PFU/mL. Figure 1 shows the logarithmic virus titers in PFU/mL of the VSV samples treated with PEI-CDots at concentrations, ranging from 0.5 to 5 μg/mL with the visible light exposure and in the dark (wrapped with aluminum foil). According to the results shown, the treatment of the samples containing ~10^6 to 10^7 PFU/mL viruses with PEI-CDots at 0.5 μg/mL and the light exposure could achieve the meaningful inactivation of ~2 log of VSVs, whereas a complete eradication of VSVs in the samples could be achieved at a higher dot concentration of 5 μg/mL, achieving >6 log PFU reduction (Figure 1A). On the other hand, in the dark control without any light exposure, the virus titers were not meaningfully reduced regardless of CDots concentrations used in the treatment. The results reaffirm the necessity of visible light activation in CDots' antiviral function,

https://doi.org/10.1021/acsabm.2c00153
ACS Appl. Bio Mater. 2022, 5, 3158−3166

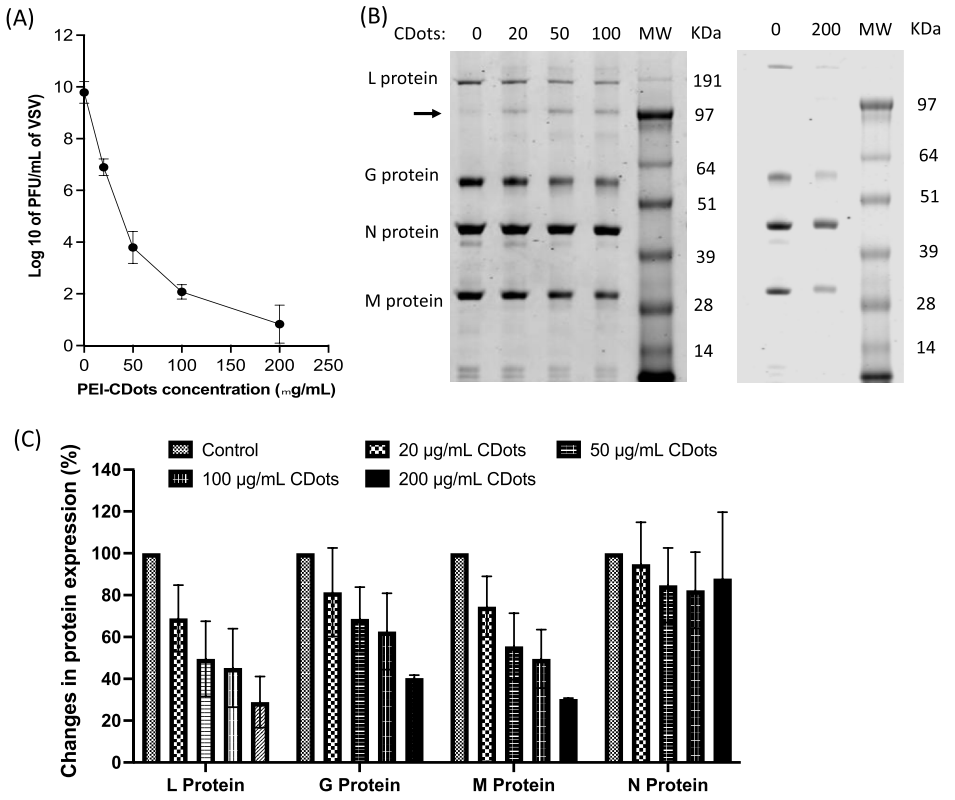

Figure 2. (A) Viral titer reduction in VSV samples containing higher viral titers (10^9 to 10^{10} PFU/mL) upon 1 h treatment with PEI-CDots at higher concentrations with visible light activation. (B) Images of SDS-PAGE gel for the analysis of VSV structural proteins upon the treatments with different concentrations of CDots under visible light for 1 h. (C) Quantitative analytic results of the changes in the expression of the five structural proteins in VSVs upon CDots treatments.

further supporting the conclusions from previous investigations on the antimicrobial activities of CDots with visible/natural light.[23−25] Moreover, as shown in Figure 1B on the dependence on the treatment time, the treatment with 5 μg/mL PEI-CDots coupled with visible light could inactivate ∼3 log VSVs in 15 min, ∼5 log in 30 min, ∼6 log in 45 min, and all viruses in the tested samples in 60 min. These results suggest that CDots with visible light activation are highly effective for the inactivation of VSVs in a dot concentration- and treatment time-dependent manner (Figure 1A,B), which is consistent with its antiviral activities toward other virus models[29,31] and its antibacterial functions toward various bacteria reported in our previous studies.[23−25] Besides, CDots' antimicrobial activity is generally affected by several other factors, including light intensity and CDots properties (such as quantum yield, surface charge, and surface passivation layer).[23,24,41] In the case of this study, the PEI-CDots in aqueous solution of near neutral pH with their surface groups $-NH_3^+$ are positively charged, which make them favorable to interactions with generally negative charged virus particles. In the future, for practical applications, other factors, such as organic loads or physical components on the applied targets, that may influence the efficiency of CDots' antimicrobial activity, also need to be investigated.

Damages to VSV Viral Structural Proteins by CDots Treatment. On the mechanistic insight into the virus inactivation, the degradation of the viral proteins was examined. The VSV structure is composed of a nucleocapsid surrounded by the viral envelope. The envelope is a lipid bilayer derived from the host cell and contains trimmers of a single type of an integral glycoprotein—G protein, which mediates virus entry into the target cell through endocytosis and catalyzes the fusion of viral and endosomal membranes, an essential step of infection.[42] The nucleocapsid consists of the RNA genome tightly associated with nucleoprotein (N). The viral genomic RNA is completely encapsulated by the nucleocapsid (N) protein, forming the N-RNA complex. The viral genomic RNA depends on the viral RNA-dependent RNA polymerase, which is a complex formed by the large polymerase protein (L) and the phosphoprotein (P), to replicate.[43] The complex is tightly bound to N-RNA to form the RNP complex. This RNP complex is further surrounded by the matrix protein (M) and viral envelope, namely, that the M protein is located between the envelope inner surface and nucleocapsid.[44] Our examination was to determine how the five structural proteins of the virus were affected by the CDots treatment based on SDS-PAGE analyses.

In the experiments, higher titers of VSVs and correspondingly higher CDots concentrations were used in the treatment, in order to collect sufficient amounts of proteins for analyses. Briefly, VSV samples containing ∼10^9 to 10^{10} PFU/mL were treated with 20, 50, 100, and 200 μg/mL PEI-CDots under the visible light for 1 h, with the samples without PEI-CDots as controls. The plaque assay results (Figure 2A) indicated that the VSVs were mostly inactivated upon 1 h treatment with 200 μg/mL PEI-CDots under visible light, with ∼8.7 log reduction, while 1 h treatment with 20, 50, and 100 μg/mL PEI-CDots also significantly reduced the viral titers by ∼3.1, ∼6.2, and ∼8.0 log, respectively. Therefore, all of these treatments inactivated more than 99.9% of the viruses in the samples. For

https://doi.org/10.1021/acsabm.2c00153
ACS Appl. Bio Mater. 2022, 5, 3158−3166

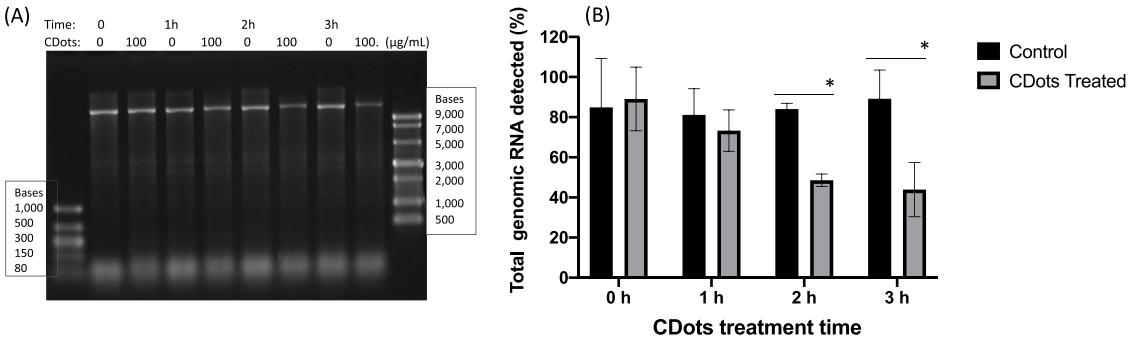

Figure 3. (A) Image of the electrophoresis gel for the analysis of VSV genomic RNA of the CDots-treated VSVs samples and the controls and (B) quantitative analysis results of the VSV genomic RNA degradation upon the treatment with 100 μg/mL PEI-CDots with visible light activation for 1−3 h. Multiple unpaired *t*-test was performed between the controls and CDots-treated samples, * indicates significant difference with $p < 0.05$.

protein analysis, after 1 h treatment, viral proteins were extracted and quantified. Aliquots of 5 μg of total protein from treated or untreated samples were loaded for SDS-PAGE, followed by Coomassie blue staining. Figure 2B shows the bands of the proteins on the (4−12%) SDS-PAGE gel, with the observation of four of the five structural proteins. According to the pattern of protein bands and the relative positions reported in the literature,[22,38,45] the four observed bands should correspond to the L protein (241 kDa), the G protein (55 kDa), the N protein (47 kDa), and the M protein (26 kDa). The minor deviation for some of the bands not at the exact full sizes as referenced to the ladder might be due to some minor truncations induced during CDots treatment. Nevertheless, the results clearly show the quantitative degradation of the structural proteins upon the treatments with different concentrations of PEI-CDots, in reference to the protein levels in untreated control VSV samples. As shown in Figure 2C, the L protein in the VSV polymerase complex and the M protein were similarly sensitive to the CDots treatment and the increasing PEI-CDots concentration used in the treatment, with the degradation of ∼25−30% after 1 h treatment with 20 μg/mL PEI-CDots and 70% after 1 h treatment with 200 μg/mL PEI-CDots. The G protein was somewhat less sensitive to the CDots treatment, degrading 20 and ∼60% after 1 h treatment with 20 and 200 μg/mL PEI-CDots, respectively. The N protein was apparently the most resistant to the CDots treatment, exhibiting no significant degradation in all samples treated by different concentrations of PEI-CDots. In the literature, there have been reports on similar degradations of the various VSV structural proteins in other physical and chemical inactivation approaches.[22,38] However, despite the resistance of the N protein in VSV, the damage/degradation to any of the five structural proteins is lethal to the virus.[22]

In protein assay, as shown in Figure 2B, there was a band above the G-protein band (indicated by an arrow at approximately 130 kDa) for CDots-treated VSV samples, which was more evident with the treatment at higher PEI-CDots concentrations. The result is similar to what was reported previously in SDS-PAGE analysis of VSV proteins after the treatment with porphyrins and derivatives.[38] According to Cruz-Oliveira et al.,[38] this band likely corresponds to large complexes of G glycoprotein. Thus, such a band in our results may suggest that the CDots treatment could induce VSV G glycoprotein cross-linking in the virus envelope, which might contribute to the loss of infectivity of CDots-treated VSV, as G-protein mediates the virus entry into its host cell. In fact, the protein cross-linking was considered as the primary inactivation mechanism in previous studies on VSV inactivation by photodynamic agents, porphyrin derivatives and phthalocyanines.[46] With the CDots treatment, other than the protein cross-linking might be contributing mechanistically, however, the degradation of the L, P, and M proteins also suggested damages deep into the VSV envelope. It is known that such damages of the viral proteins could lead to changes to host receptor recognition sites on the virus capsid/envelope and inhibit the host receptor attachment, thereby resulting in the inability of the virus to infect the host cell.[47]

Degradation of Viral Genomic RNA. VSV is a non-segmented negative-sense RNA virus, with a genome size of 11 kb. It is lethal to the virus when the viral RNA genome is damaged or degraded. Figure 3 shows the image of the electrophoresis gel for the analysis of the VSV genomic RNA extracted from CDots-treated samples and control samples containing high titer VSVs (∼10^9 to 10^{10} PFU/mL). The remaining amount of the VSV genomic RNA decreased with the treatment at the same PEI-CDots concentration of 100 μg/mL but increasing treatment time from 1, 2 to 3 h, while the amount of viral genomic RNA in the control samples was largely unchanged. However, with the VSV genomic RNA completely encapsidated by the N protein, some could be still protected if the N protein was not completely degraded. Indeed, after 3 h treatment with 100 μg/mL PEI-CDots, there was about half VSV genomic RNA still intact according to the gel assay. Nevertheless, with the serious damage to or degradation of genomic RNA and the structural proteins, the infectivity of the VSVs is clearly disabled.

Scavenging ROS in CDots Treatments. The potent antimicrobial function of light-activated CDots is attributed to their unique photoexcited state properties and processes.[29,30] In the mechanistic framework of photoexcited CDots, there are two sets of highly reactive species that could both contribute to the observed antimicrobial activities. One is the separated radical cation and radical anion pairs generated in the initial ultrafast charge transfer and separation following the photoexcitation of CDots, and the other is the traditional ROS generated in the emissive excited states formed by the radiative recombination of separated redox pairs.[29,30] The former is much shorter lived than the latter, generally beyond the limit of diffusional quenching, and as a result the presence of conventional ROS scavengers in the CDots treatment has not been able to protect the overwhelming majority of the bacterial cells from the killing by the light-activated CDots.[29,30]

https://doi.org/10.1021/acsabm.2c00153
ACS Appl. Bio Mater. 2022, 5, 3158−3166

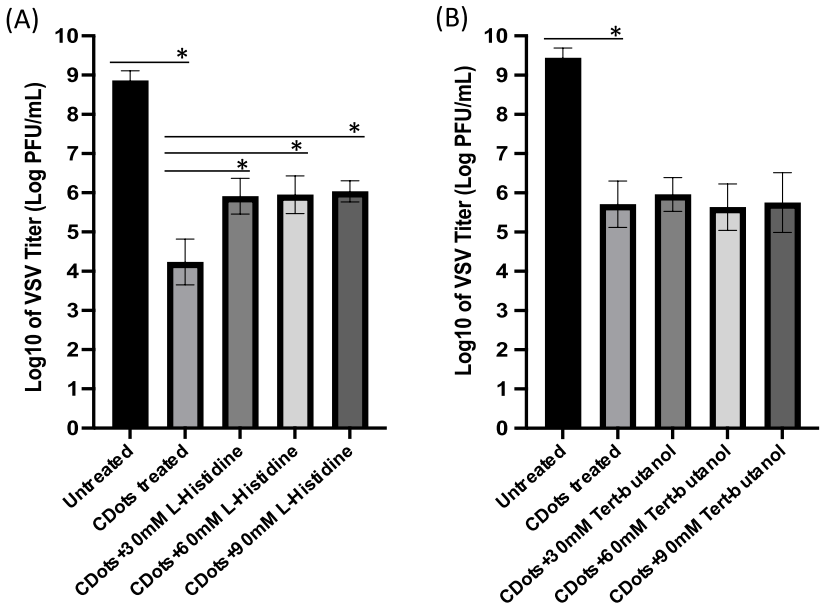

Figure 4. Effects of scavengers L-histidine (A) and *tert*-butanol (B) on the antiviral function of CDots toward VSVs. The concentrations of the respective scavengers used in the experiments were 30, 60, and 90 mM. VSV samples: 10^8 to 10^9 PFU/mL; treatment: 20 μg/mL PEI-CDots under visible light illumination for 1 h, in the presence or absence of the tested scavenger. * indicates significant difference with $p < 0.05$.

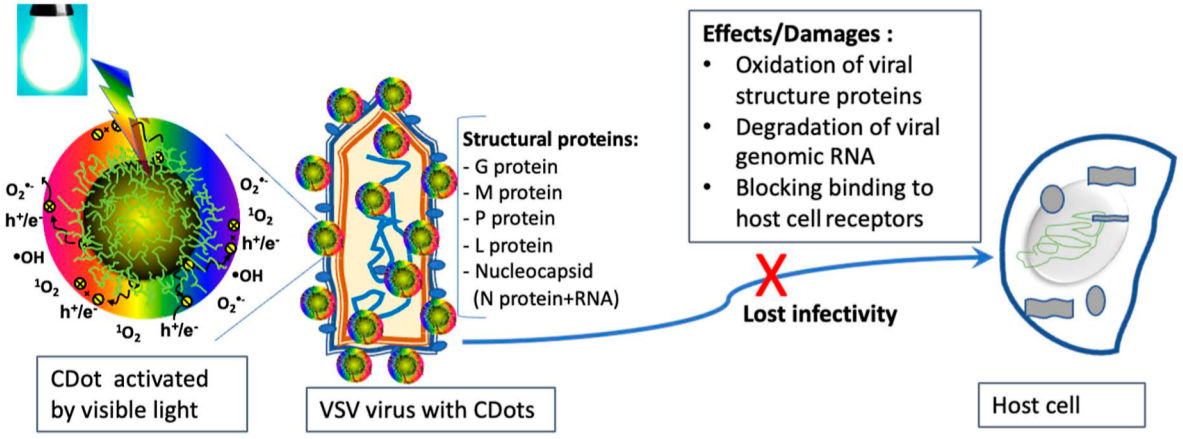

Figure 5. Scheme of the mechanistic aspects of CDots' antiviral activity and the possible damages/effects on virus particles that led to the loss of viral infectivity.

The outcome was similar from our scavenging experiments described as follows.

In the experiments, ROS scavengers, L-histidine and *tert*-butanol, were added to the samples in CDots treatments to target the singlet molecular oxygen ($^1O_2$) and hydroxyl radicals ($^\bullet$OH), respectively, because these scavengers have been widely used with significant success in the study of photodynamic effects by organic dyes.[48,49] For both scavengers, their concentrations varied from 30 to 90 mM. Figure 4A, B shows the quenching effects of L-histidine or *tert*-butanol on the inactivation of VSVs by PEI-CDots treatment. The treatment with 20 μg/mL PEI-CDots under visible light to the samples containing ~10^9 PFU/mL VSVs resulted in ~3 log reduction in viral titers in the presence of 30−90 mM L-histidine versus ~4.5 log reduction in viral titers without the scavenger (Figure 4A), hardly effective in the protective effect (e.g., only limited protection in the presence of the scavenger). Figure 4B shows that the addition and presence of up to 90 mM *tert*-butanol in CDots treatment with visible light resulted in no protective effect on VSV from the action of CDots, with the same reductions in viral titers without *tert*-butanol. The result is the same as what was observed in the scavenging experiments on protecting bacterial cells from the killing action of light-activated CDots.[30]

Interestingly, as shown in Figure 4A, the quenching effect of L-histidine apparently reached a plateau when the L-histidine concentration increased from 30 to 90 mM. On the reduction of viral titers in the samples from the initial ~8.1×10^8 PFU/mL, the reduction was more than 99.99% to ~2.7×10^4 PFU/mL after the treatment with 20 μg/mL under visible light, whereas with same CDots treatment in the presence of L-histidine, the reduction was ~98.03% to ~1.6×10^7 PFU/mL, not a significant protection effect and no more increase in the protection when the amount of the scavenger was tripled. It might be speculated that mechanistically L-histidine could only quench the longer lived ROS generated in the emissive excited states of the CDots, with the saturation of the quenching reached at a certain L-histidine concentration. More generally,

https://doi.org/10.1021/acsabm.2c00153
ACS Appl. Bio Mater. 2022, 5, 3158−3166

the fact that the killing action of light-activated CDots, on bacterial pathogens[30] and viruses alike could not be quenched by established ROS scavengers distinguishes CDots from classical dye photosensitizers as a unique class of highly potent antimicrobial agents.

Mechanistic Implications. Mechanistically, the antiviral activity of light-activated CDots may be understood, as illustrated in Figure 5. Upon photoexcitation of CDots with exposure to visible light, there is the generation of two sets of highly reactive species, the separated redox pairs (h^+/e^-) trapped at the abundant surface defect sites of the small carbon nanoparticles in CDots that are effectively passivated by the organic functionalization and the classical ROS associated with the emissive excited states formed from the recombination of the separated redox pairs.[29,30] These highly reactive species collectively induce diverse damages/effects on the virus particles, including the oxidation of viral proteins, the degradation of viral genomic RNA, and possibly the blocking of viral binding to host cell receptors.[31,32] Such damages/effects probably disable the recognition sites on the viral capsid/envelope and inhibit the attachment and the entry to host cells, resulting in the loss of viral infectivity to its host cells. Ultimately, the outcome is the highly effective and efficient inactivation of the virus by CDots coupled with visible light exposure. Among challenges and opportunities in further mechanistic elucidation of the antiviral function and antimicrobial properties in general of light-activated CDots may include a more detailed understanding of the separated redox pairs and their interactions with and action against the target virus/bacteria, probably by a direct ultrafast spectroscopy probing and the exploration of other quenching strategies, with the results thus obtained to be correlated with the antimicrobial outcomes. Apparently, broad multidisciplinary efforts are required.

CONCLUSIONS

As demonstrated in this study, CDots with visible light exhibited excellent antiviral activity to enveloped VSVs, effectively inactivating the virus by diminishing their infectivity to host cells. The treatment of CDots with visible light damaged the viral structural proteins and degraded their genomic RNA. The results added further evidence for the broad-spectrum antiviral function of CDots toward viruses of diverse structures. Moreover, the visible light activation of CDots for the effective antiviral function is also fully compatible with the human friendly environment, avoiding the known hazards associated with UV light. Thus, promising applications of the approach in the disinfection of viruses during their transmission route may be envisaged. On mechanistic understandings, the reported results established the association of the inactivation with the damages of viral structural proteins and the degradation of genomic RNA, demonstrated the unique characteristics of the killing action little affected by the presence of widely used ROS scavengers, and sketched out a framework for further investigations on the reactive species in photoexcited CDots and their functions responsible for the observed antimicrobial activities.

ASSOCIATED CONTENT

Supporting Information

The Supporting Information is available free of charge at https://pubs.acs.org/doi/10.1021/acsabm.2c00153.

Additional experimental details for preparation of PEI-CDots and the results of characterizations and properties of PEI-CDots, including NMR data, TEM and SEM images, and adsorption spectra (PDF)

AUTHOR INFORMATION

Corresponding Authors

Ya-Ping Sun − *Department of Chemistry, Clemson University, Clemson, South Carolina 29634, United States;* orcid.org/0000-0001-8593-5769; Email: syaping@clemson.edu

Liju Yang − *Biomanufacturing Research Institute and Technology Enterprise (BRITE) and Department of Pharmaceutical Sciences, North Carolina Central University, Durham, North Carolina 27707, United States;* orcid.org/0000-0002-4776-7597; Email: lyang@nccu.edu

Authors

Audrey F. Adcock − *Biomanufacturing Research Institute and Technology Enterprise (BRITE) and Department of Pharmaceutical Sciences, North Carolina Central University, Durham, North Carolina 27707, United States*

Ping Wang − *Department of Chemistry, Clemson University, Clemson, South Carolina 29634, United States*

Isaiah S. Ferguson − *Biomanufacturing Research Institute and Technology Enterprise (BRITE) and Department of Pharmaceutical Sciences, North Carolina Central University, Durham, North Carolina 27707, United States*

Somtochukwu C. Obu − *Biomanufacturing Research Institute and Technology Enterprise (BRITE) and Department of Pharmaceutical Sciences, North Carolina Central University, Durham, North Carolina 27707, United States*

Complete contact information is available at: https://pubs.acs.org/10.1021/acsabm.2c00153

Notes

The authors declare no competing financial interest.

ACKNOWLEDGMENTS

Financial support from NSF grants 1855905, 2102021, and 2102056 is gratefully acknowledged.

REFERENCES

(1) Moriyama, M.; Hugentobler, W. J.; Iwasaki, A. Seasonality of Respiratory Viral Infections. *Annu. Rev. Virol.* **2020**, *7*, 83−101.

(2) Li, Q.; Guan, X.; Wu, P.; Wang, X.; Zhou, L.; Tong, Y.; Ren, R.; Leung, K. S. M.; Lau, E. H. Y.; Wong, J. Y.; Xing, X.; Xiang, N.; Wu, Y.; Li, C.; Chen, Q.; Li, D.; Liu, T.; Zhao, J.; Liu, M.; Tu, W.; Chen, C.; Jin, L.; Yang, R.; Wang, Q.; Zhou, S.; Wang, R.; Liu, H.; Luo, Y.; Liu, Y.; Shao, G.; Li, H.; Tao, Z.; Yang, Y.; Deng, Z.; Liu, B.; Ma, Z.; Zhang, Y.; Shi, G.; Lam, T. T. Y.; Wu, J. T.; Gao, G. F.; Cowling, B. J.; Yang, B.; Leung, G. M.; Feng, Z. Early Transmission Dynamics in Wuhan, China, of Novel Coronavirus-Infected Pneumonia. *N. Engl. J. Med.* **2020**, *382*, 1199−1207.

(3) Paules, C. I.; Marston, H. D.; Fauci, A. S. Coronavirus Infections-More Than Just the Common Cold. *JAMA* **2020**, *323*, 707−708.

(4) Lauring, A. S.; Malani, P. N. Variants of SARS-CoV-2. *JAMA* **2021**, *326*, 880.

(5) Molinari, N.-A. M.; Ortega-Sanchez, I. R.; Messonnier, M. L.; Thompson, W. W.; Wortley, P. M.; Weintraub, E.; Bridges, C. B. The annual impact of seasonal influenza in the US: measuring disease burden and costs. *Vaccine* **2007**, *25*, 5086−5096.

(6) Lozano, R.; Naghavi, M.; Foreman, K.; Lim, S.; Shibuya, K.; Aboyans, V.; Abraham, J.; Adair, T.; Aggarwal, R.; Ahn, S. Y.; AlMazroa, M. A.; Alvarado, M.; Anderson, H. R.; Anderson, L. M.; Andrews, K. G.; Atkinson, C.; Baddour, L. M.; Barker-Collo, S.; Bartels, D. H.; Bell, M. L.; Benjamin, E. J.; Bennett, D.; Bhalla, K.; Bikbov, B.; Abdulhak, A. B.; Birbeck, G.; Blyth, F.; Bolliger, I.; Boufous, S.; Bucello, C.; Burch, M.; Burney, P.; Carapetis, J.; Chen, H.; Chou, D.; Chugh, S. S.; Coffeng, L. E.; Colan, S. D.; Colquhoun, S.; Colson, K. E.; Condon, J.; Connor, M. D.; Cooper, L. T.; Corriere, M.; Cortinovis, M.; de Vaccaro, K. C.; Couser, W.; Cowie, B. C.; Criqui, M. H.; Cross, M.; Dabhadkar, K. C.; Dahodwala, N.; De Leo, D.; Degenhardt, L.; Delossantos, A.; Denenberg, J.; Des Jarlais, D. C.; Dharmaratne, S. D.; Dorsey, E. R.; Driscoll, T.; Duber, H.; Ebel, B.; Erwin, P. J.; Espindola, P.; Ezzati, M.; Feigin, V.; Flaxman, A. D.; Forouzanfar, M. H.; Fowkes, F. G. R.; Franklin, R.; Fransen, M.; Freeman, M. K.; Gabriel, S. E.; Gakidou, E.; Gaspari, F.; Gillum, R. F.; Gonzalez-Medina, D.; Halasa, Y. A.; Haring, D.; Harrison, J. E.; Havmoeller, R.; Hay, R. J.; Hoen, B.; Hotez, P. J.; Hoy, D.; Jacobsen, K. H.; James, S. L.; Jasrasaria, R.; Jayaraman, S.; Johns, N.; Karthikeyan, G.; Kassebaum, N.; Keren, A.; Khoo, J.-P.; Knowlton, L. M.; Kobusingye, O.; Koranteng, A.; Krishnamurthi, R.; Lipnick, M.; Lipshultz, S. E.; Ohno, S. L.; Mabweijano, J.; MacIntyre, M. F.; Mallinger, L.; March, L.; Marks, G. B.; Marks, R.; Matsumori, A.; Matzopoulos, R.; Mayosi, B. M.; McAnulty, J. H.; McDermott, M. M.; McGrath, J.; Memish, Z. A.; Mensah, G. A.; Merriman, T. R.; Michaud, C.; Miller, M.; Miller, T. R.; Mock, C.; Mocumbi, A. O.; Mokdad, A. A.; Moran, A.; Mulholland, K.; Nair, M. N.; Naldi, L.; Narayan, K. M. V.; Nasseri, K.; Norman, P.; O'Donnell, M.; Omer, S. B.; Ortblad, K.; Osborne, R.; Ozgediz, D.; Pahari, B.; Pandian, J. D.; Rivero, A. P.; Padilla, R. P.; Perez-Ruiz, F.; Perico, N.; Phillips, D.; Pierce, K.; Pope, C. A.; Porrini, E.; Pourmalek, F.; Raju, M.; Ranganathan, D.; Rehm, J. T.; Rein, D. B.; Remuzzi, G.; Rivara, F. P.; Roberts, T.; De León, F. R.; Rosenfeld, L. C.; Rushton, L.; Sacco, R. L.; Salomon, J. A.; Sampson, U.; Sanman, E.; Schwebel, D. C.; Segui-Gomez, M.; Shepard, D. S.; Singh, D.; Singleton, J.; Sliwa, K.; Smith, E.; Steer, A.; Taylor, J. A.; Thomas, B.; Tleyjeh, I. M.; Towbin, J. A.; Truelsen, T.; Undurraga, E. A.; Venketasubramanian, N.; Vijayakumar, L.; Vos, T.; Wagner, G. R.; Wang, M.; Wang, W.; Watt, K.; Weinstock, M. A.; Weintraub, R.; Wilkinson, J. D.; Woolf, A. D.; Wulf, S.; Yeh, P.-H.; Yip, P.; Zabetian, A.; Zheng, Z.-J.; Lopez, A. D.; Murray, C. J. Global and regional mortality from 235 causes of death for 20 age groups in 1990 and 2010: a systematic analysis for the Global Burden of Disease Study 2010. *Lancet* **2012**, *380*, 2095−2128.

(7) D'Souza, D. H.; Su, X. Efficacy of Chemical Treatments Against Murine Norovirus, Feline Calicivirus, and MS2 Bacteriophage. *Foodborne Pathog. Dis.* **2010**, *7*, 319−326.

(8) D'Souza, D. H.; Su, X.; Roach, A.; Harte, F. High-Pressure Homogenization for the Inactivation of Human Enteric Virus Surrogates. *J. Food Protect.* **2009**, *72*, 2418−2422.

(9) Duizer, E.; Bijkerk, P.; Rockx, B.; de Groot, A.; Twisk, F.; Koopmans, M. Inactivation of caliciviruses. *Appl. Environ. Microbiol.* **2004**, *70*, 4538−4543.

(10) Escudero-Abarca, B. I.; Rawsthorne, H.; Goulter, R. M.; Suh, S. H.; Jaykus, L. A. Molecular methods used to estimate thermal inactivation of a prototype human norovirus: More heat resistant than previously believed? *Food Microbiol.* **2014**, *41*, 91−95.

(11) Girard, M.; Ngazoa, S.; Mattison, K.; Jean, J. Attachment of Noroviruses to Stainless Steel and Their Inactivation, Using Household Disinfectants. *J. Food Protect.* **2010**, *73*, 400−404.

(12) Kingsley, D. H.; Vincent, E. M.; Meade, G. K.; Watson, C. L.; Fan, X. Inactivation of human norovirus using chemical sanitizers. *Int. J. Food Microbiol.* **2014**, *171*, 94−99.

(13) Lee, J. E.; Ko, G. Norovirus and MS2 inactivation kinetics of UV-A and UV-B with and without TiO_2. *Water Res.* **2013**, *47*, 5607−5613.

(14) Macinga, D. R.; Sattar, S. A.; Jaykus, L.-A.; Arbogast, J. W. Improved inactivation of nonenveloped enteric viruses and their surrogates by a novel alcohol-based hand sanitizer. *Appl. Environ. Microbiol.* **2008**, *74*, 5047−5052.

(15) Vimont, A.; Fliss, I.; Jean, J. Efficacy and Mechanisms of Murine Norovirus Inhibition by Pulsed-Light Technology. *Appl. Environ. Microbiol.* **2015**, *81*, 2950−2957.

(16) Bertrand, I.; Schijven, J. F.; Sánchez, G.; Wyn-Jones, P.; Ottoson, J.; Morin, T.; Muscillo, M.; Verani, M.; Nasser, A.; de Roda Husman, A. M.; Myrmel, M.; Sellwood, J.; Cook, N.; Gantzer, C. The impact of temperature on the inactivation of enteric viruses in food and water: a review. *J. Appl. Microbiol.* **2012**, *112*, 1059−1074.

(17) Bozkurt, H.; D'Souza, D. H.; Davidson, P. M. Thermal Inactivation of Human Norovirus Surrogates in Spinach and Measurement of Its Uncertainty. *J. Food Protect.* **2014**, *77*, 276−283.

(18) Lou, F.; Huang, P.; Neetoo, H.; Gurtler, J. B.; Niemira, B. A.; Chen, H.; Jiang, X.; Li, J. High-Pressure Inactivation of Human Norovirus Virus-Like Particles Provides Evidence that the Capsid of Human Norovirus Is Highly Pressure Resistant. *Appl. Environ. Microbiol.* **2012**, *78*, 5320−5327.

(19) Grove, S. F.; Forsyth, S.; Wan, J.; Coventry, J.; Cole, M.; Stewart, C. M.; Lewis, T.; Ross, T.; Lee, A. Inactivation of hepatitis A virus, poliovirus and a norovirus surrogate by high pressure processing. *Innovative Food Sci. Emerging* **2008**, *9*, 206−210.

(20) Li, X.; Ye, M.; Neetoo, H.; Golovan, S.; Chen, H. Pressure inactivation of Tulane virus, a candidate surrogate for human norovirus and its potential application in food industry. *Int. J. Food Microbiol.* **2013**, *162*, 37−42.

(21) Huang, R.; Li, X.; Huang, Y.; Chen, H. Strategies to enhance high pressure inactivation of murine norovirus in strawberry puree and on strawberries. *Int. J. Food Microbiol.* **2014**, *185*, 1−6.

(22) Feng, K.; Divers, E.; Ma, Y.; Li, J. Inactivation of a Human Norovirus Surrogate, Human Norovirus Virus-Like Particles, and Vesicular Stomatitis Virus by Gamma Irradiation. *Appl. Environ. Microbiol.* **2011**, *77*, 3507−3517.

(23) Abu Rabe, D. I.; Mohammed, O. O.; Dong, X.; Patel, A. K.; Overton, C. M.; Tang, Y.; Katharíou, S.; Sun, Y.-P.; Yang, L. Carbon dots for highly effective photodynamic inactivation of multidrug-resistant bacteria. *Adv. Mater.* **2020**, *1*, 321−325.

(24) Al Awak, M. M.; Wang, P.; Wang, S.; Tang, Y.; Sun, Y.-P.; Yang, L. Correlation of Carbon Dots' Light-Activated Antimicrobial Activities and Fluorescence Quantum Yield. *RSC Adv.* **2017**, *7*, 30177−30184.

(25) Meziani, M. J.; Dong, X.; Zhu, L.; Jones, L. P.; LeCroy, G. E.; Yang, F.; Wang, S.; Wang, P.; Zhao, Y.; Yang, L.; Tripp, R. A.; Sun, Y.-P. Visible-Light-Activated Bactericidal function of carbon dots 'Quantum" dots. *ACS Appl. Mater. Interfaces* **2016**, *8*, 10761−10766.

(26) Garg, P.; Sangam, S.; Kochhar, D.; Pahari, S.; Kar, C.; Mukherjee, M. Exploring the role of triazole functionalized heteroatom co-doped carbon quantum dots against human coronaviruses. *Nano Today* **2020**, *35*, 101001.

(27) Innocenzi, P.; Stagi, L. Carbon-based antiviral nanomaterials: graphene, C-dots, and fullerenes. A perspective. *Chem. Sci.* **2020**, *11*, 6606−6622.

(28) Huang, S.; Gu, J.; Ye, J.; Fang, B.; Wan, S.; Wang, C.; Ashraf, U.; Li, Q.; Wang, X.; Shao, L.; Song, Y.; Zheng, X.; Cao, F.; Cao, S. Benzoxazine monomer derived carbon dots as a broad-spectrum agent to block viral infectivity. *J. Colloid Interface Sci.* **2019**, *542*, 198−206.

(29) Dong, X.; Edmondson, R.; Yang, F.; Tang, Y.; Wang, P.; Sun, Y.-P.; Yang, L. Carbon dots for effective photodynamic inactivation of virus. *RSC Adv.* **2020**, *10*, 33944−33954.

(30) Dong, X.; Ge, L.; Abu Rabe, D. I.; Mohammed, O. O.; Wang, P.; Tang, Y.; Katharíou, S.; Yang, L.; Sun, Y.-P. Photoexcited state properties and antibacterial activities of carbon dots relevant to mechanistic features and implications. *Carbon* **2020**, *170*, 137−145.

(31) Dong, X.; Moyer, M. M.; Yang, F.; Sun, Y.-P.; Yang, L. Carbon Dots' Antiviral Functions Against Noroviruses. *Sci. Rep.* **2017**, *7*, 519.

(32) Barras, A.; Pagneux, Q.; Sane, F.; Wang, Q.; Boukherroub, R.; Hober, D.; Szunerits, S. High Efficiency of Functional Carbon Nanodots as Entry Inhibitors of Herpes Simplex Virus Type 1. *ACS Appl. Mater. Interfaces* **2016**, *8*, 9004−9013.

https://doi.org/10.1021/acsabm.2c00153
ACS Appl. Bio Mater. 2022, 5, 3158−3166

(33) Ivanova, P. T.; Myers, D. S.; Milne, S. B.; McClaren, J. L.; Thomas, P. G.; Brown, H. A. Lipid composition of viral envelope of three strains of influenza virus - not all viruses are created equal. *ACS Infect. Dis.* **2015**, *1*, 399−452.
(34) Wisskirchen, K.; Lucifora, J.; Michler, T.; Protzer, U. New pharmacological strategies to fight enveloped viruses. *Trends Pharmacol. Sci.* **2014**, *35*, 470−478.
(35) Vigant, F.; Santos, N. C.; Lee, B. Broad-spectrum antivirals against viral fusion. *Nat. Rev. Microbiol.* **2015**, *13*, 426−437.
(36) Di Mascio, P.; Martinez, G. R.; Miyamoto, S.; Ronsein, G. E.; Medeiros, M. H. G.; Cadet, J. Singlet Molecular Oxygen Reactions with Nucleic Acids, Lipids, and Proteins. *Chem. Rev.* **2019**, *119*, 2043−2086.
(37) Bacellar, I. O. L.; Baptista, M. S. Mechanisms of Photosensitized Lipid Oxidation and Membrane Permeabilization. *ACS Omega* **2019**, *4*, 21636−21646.
(38) Cruz-Oliveira, C.; Almeida, A. F.; Freire, J. M.; Caruso, M. B.; Morando, M. A.; Ferreira, V. N. S.; Assuncao-Miranda, I.; Gomes, A. M. O.; Castanho, M. A. R. B.; Da Poian, A. T. Mechanisms of Vesicular Stomatitis Virus Inactivation by Protoporphyrin IX, Zinc-Protoporphyrin IX, and Mesoporphyrin IX. *Antimicrob. Agents Chemother.* **2017**, *61*, No. e00053-17.
(39) LeCroy, G. E.; Sonkar, S. K.; Yang, F.; Veca, L. M.; Wang, P.; Tackett, K. N., II; Yu, J.-J.; Vasile, E.; Qian, H.; Liu, Y.; Luo, P.; Sun, Y.-P. Toward structurally defined carbon dots as ultracompact fluorescent probes. *ACS Nano* **2014**, *8*, 4522−4529.
(40) Yang, F.; LeCroy, G. E.; Wang, P.; Liang, W.; Chen, J.; Fernando, K. A. S.; Bunker, C. E.; Qian, H.; Sun, Y.-P. Functionalization of Carbon Nanoparticles and Defunctionalization-Toward Structural and Mechanistic Elucidation of Carbon "Quantum" Dots. *J. Phys. Chem. C* **2016**, *120*, 25604−25611.
(41) Abu Rabe, D. I.; Al Awak, M. M.; Yang, F.; Okonjo, P. A.; Dong, X.; Teisl, L. R.; Wang, P.; Tang, Y.; Pan, N.; Sun, Y.-P.; Yang, L. The dominant role of surface functionalization in carbon dots' photo-activated antibacterial activity. *Int. J. Nanomed.* **2019**, *14*, 2655−2665.
(42) Carneiro, F. A.; Stauffer, F.; Lima, C. S.; Juliano, M. A.; Juliano, L.; Da Poian, A. T. Membrane fusion induced by vesicular stomatitis virus depends on histidine protonation. *J. Biol. Chem.* **2003**, *278*, 13789−13794.
(43) Albertini, A. A. V.; Baquero, E.; Ferlin, A.; Gaudin, Y. Molecular and Cellular Aspects of Rhabdovirus Entry. *Viruses* **2012**, *4*, 117−139.
(44) Beilstein, F.; Obiang, L.; Raux, H.; Gaudin, Y. Characterization of the Interaction between the Matrix Protein of Vesicular Stomatitis Virus and the Immunoproteasome Subunit LMP2. *J. Virol.* **2015**, *89*, 11019−11029.
(45) Hirayama, J.; Ikebuchi, K.; Abe, H.; Kwon, K.-W.; Ohnishi, Y.; Horiuchi, M.; Shinagawa, M.; Ikuta, K.; Kamo, N.; Sekiguchi, S. Photoinactivation of virus infectivity by hypocrellin. A. *Photochem. Photobiol.* **1997**, *66*, 697−700.
(46) Lim, D.-S.; Ko, S.-H.; Kim, S.-J.; Park, Y.-J.; Park, J.-H.; Lee, W.-Y. Photoinactivation of vesicular stomatitis virus by a photodynamic agent, chlorophyll derivatives from silkworm excreta. *J. Photochem. Photobiol., B* **2002**, *67*, 149−156.
(47) Majiya, H.; Adeyemi, O. O.; Stonehouse, N. J.; Millner, P. Photodynamic inactivation of bacteriophage MS2: The A-protein is the target of virus inactivation. *J. Photochem. Photobiol., B* **2018**, *178*, 404−411.
(48) Hara, K.; Holland, S.; Woo, J. Effects of Exogenous Reactive Oxygen Species Scavengers on the Survival of Escherichia coli B23 during Exposure to UV-A radiation. *J. Exp. Microbiol. Immunol.* **2004**, *12*, 62−66.
(49) Ishiyama, K.; Nakamura, K.; Ikai, H.; Kanno, T.; Kohno, M.; Sasaki, K.; Niwano, Y. Bactericidal Action of Photogenerated Singlet Oxygen from Photosensitizers Used in Plaque Disclosing Agents. *PLoS One* **2012**, *7*, No. e37871.

https://doi.org/10.1021/acsabm.2c00153
ACS Appl. Bio Mater. 2022, 5, 3158−3166